

Effect of Zn content on the microstructures and mechanical properties of laser beam-welded ZK series magnesium alloys

Z. H. Yu · H. G. Yan · J. H. Chen ·
Y. Z. Wu

Received: 28 October 2009 / Accepted: 20 March 2010 / Published online: 2 April 2010
© Springer Science+Business Media, LLC 2010

Abstract The effect of Zn content on the microstructures and mechanical properties of laser beam welded ZK series magnesium alloys (ZK21, ZK40, and ZK60) has been studied. Owing to the lower heat input, laser beam welding can successfully be employed to weld ZK series magnesium alloys having Zn content up to 4 wt%, which are difficult to weld by means of conventional arc welding. However, ZK60 is susceptible to solidification cracking and presents a poor weldability, which may originate from the net-like distribution of more Mg₅₁Zn₂₀ precipitates along grain boundaries (GBs) in the fusion zone (FZ). With increasing Zn content, the amount and size of precipitates along GBs in the FZ increase, and the morphology of grains in the FZ adjacent to fusion boundary changes from cellular to equiaxed dendritic. The grains in the FZ of ZK40 alloy are the finest among the three alloys, whose size is only about 4.8 μm, and the ZK40-welded joint achieves the highest ultimate tensile strength of 312 MPa, which is up to 90.4% of the base metal.

Introduction

Magnesium alloys have been considered as one of the most promising lightweight materials due to low density, high specific strength, and superior properties for absorbing vibration or shock energy, insulating electromagnetic interference, etc. Their weight saving potential when used as structural materials in aircraft and automobile industries

is beneficial to fuel economy and reducing CO₂ emissions [1–3]. Compared with AZ (Mg–Al–Zn) series and the AM (Mg–Al–Mn) series magnesium alloys, ZK (Mg–Zn–Zr) series alloys are characteristics of higher strength, better stress corrosion resistance and heat-treatability [4]. However, it has been reported that magnesium alloys with Zn as the major alloying element are more difficult to be welded by conventional arc welding methods, wherein cracking occurs as a consequence of rather a wide melting range and excessive heat input [5]. Laser beam welding (LBW) and friction stir welding (FSW) can be used as alternative methods, which can mitigate the disadvantages mentioned above due to the lower heat input [6–8]. Moreover, LBW can fabricate workpieces with complicate shapes with very narrow weld bead. Therefore, LBW is assumed as an ideally preferred choice for welding ZK series magnesium alloys [9].

Up to now, a great deal of investigations have been conducted on the laser welding of the AZ, AM, Mg–Y–RE (WE), and Mg–Zn–RE (ZE) alloys [10–13], whereas only a few have been reported on ZK series magnesium alloys. Thus, the weldability of ZK alloys and the effect of major alloying element (Zn) in LBW are still unclear. In this study, LBW is adopted to weld three ZK alloys with different Zn content, i.e., ZK21, ZK40, and ZK60, and the effects of Zn content on the microstructures and mechanical properties of the welded joints are investigated. The results are expected to be a guidance to develop the high strength and weldable magnesium alloys.

Experimental

The as-rolled ZK21, ZK40, and ZK60 magnesium alloy sheets with the dimension of 120 mm × 50 mm × 2 mm

Z. H. Yu · H. G. Yan (✉) · J. H. Chen · Y. Z. Wu
College of Materials Science and Engineering, Hunan
University, 410082 Changsha, China
e-mail: mailyzh@gmail.com

Table 1 The nominal compositions and mechanical properties of the as-rolled ZK series alloys at room temperature

Alloy	Nominal compositions (wt%)			Mechanical properties		
	Zn	Zr	Mg	σ_b (MPa)	σ_s (MPa)	δ (%)
ZK21	2.3	0.45	Bal.	308 ± 5.5	225 ± 4.2	9.1 ± 5.8
ZK40	4.0	0.45	Bal.	345 ± 3.3	245 ± 6.8	11.5 ± 4.7
ZK60	6.0	0.45	Bal.	360 ± 3.2	252 ± 6.3	10.2 ± 7

were used in this study. The nominal compositions and mechanical properties of base metals are listed in Table 1. Before welding, the surfaces of each sheet were cleaned using acetone to remove grease and residue, and then abraded using abrasion wheel to avoid the influence of oxides. Welding was conducted without filler metal using a 3-kW continuous wave CO₂ laser with the following features: mode, TEM01; divergence, ≤ 2 mrad; beam diameter on focusing optic, 38 mm; and focused diameter, 0.25 mm. The focal length of the parabolic mirror used for focusing the laser beam was 127 mm. During welding, the workpiece was clamped down to fixture. The welding speed and the laser power were set at 3.0 m/min and 1200 W, respectively. The focal point of laser beam was fixed on the top surface of the workpiece. High-purity argon (99.99%) was used to protect the molten pool of the top and the back weld with the constant flow rate of 12 and 9 L/min, respectively. After welding, the obtained welds were cut, polished, and etched with a solution of 5 g tartaric acid (C₄H₆O₆) + 100 mL water for microstructural examination by optical

microscopy (OM, Leitz MM-6). The precipitates in the FZ were analyzed using X-ray diffraction (XRD, SIEMENS D-5000) applying monochromatic CuK α radiation with wavelength of 0.15406 nm, current of 35 mA, and voltage of 40 kV, transmission electron microscope (TEM, JOM-3010) with EDS, and scanning electron microscopy using backscattering electrons (SEM, FEI QUANTA-200). The mechanical properties were measured by the Instron 8032 tensile machine. The tensile fracture surfaces were observed by SEM using secondary electrons. The microhardness testing was conducted on a HV hardness tester (401MVA). Figure 1 gives the schematic drawings of the specimens.

Results and discussion

Microstructures of the joints

The microstructures of the ZK21-, ZK40-, and ZK60-welded joints are shown in Fig. 2. As seen from Fig. 2a, c, and e, the Zn content significantly affects the microstructures of partial melted zone (PMZ) adjacent to the fusion boundary. No apparent liquation is existent in the zone left to the fusion boundary in ZK21, while obvious liquation is detected in both ZK40 and ZK60. As shown in Fig. 2c and e, the grain boundaries (GBs) exhibit the lighter-etching in color, and the liquation for ZK60 is more extensive. It is reported that the extensive liquation may lead to liquation cracking in the PMZ during welding [5]. Besides, it can also be seen that there are a few dark-etching particles distributing within grains in the PMZ of ZK40 and ZK60, indicating that

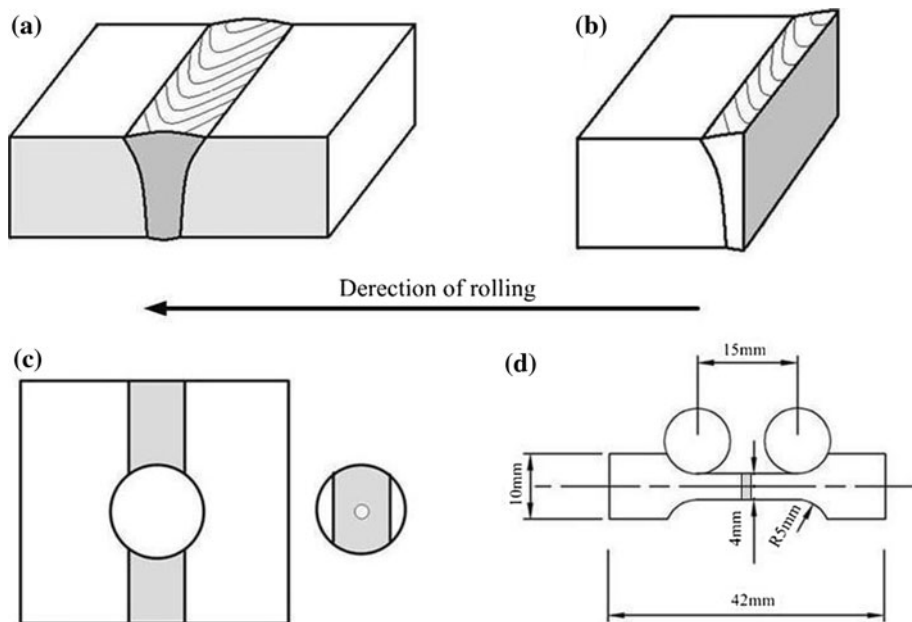
Fig. 1 Schematic drawings of the specimens extracted from the fusion zone: **a** specimen for OM and microhardness, **b** specimen for XRD, **c** specimen for TEM, and **d** specimen for tensile test

Fig. 2 Microstructures of the welded joints: **a, b** ZK21; **c, d** ZK40; **e, f** ZK60

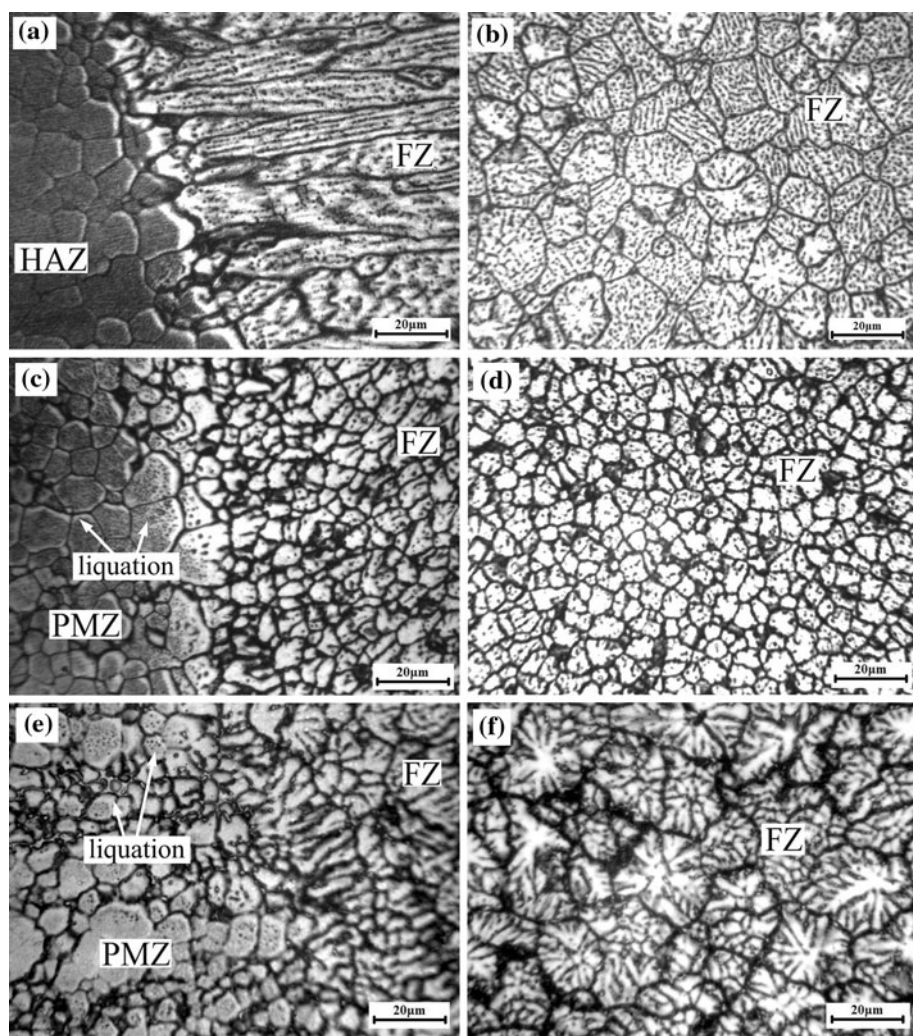
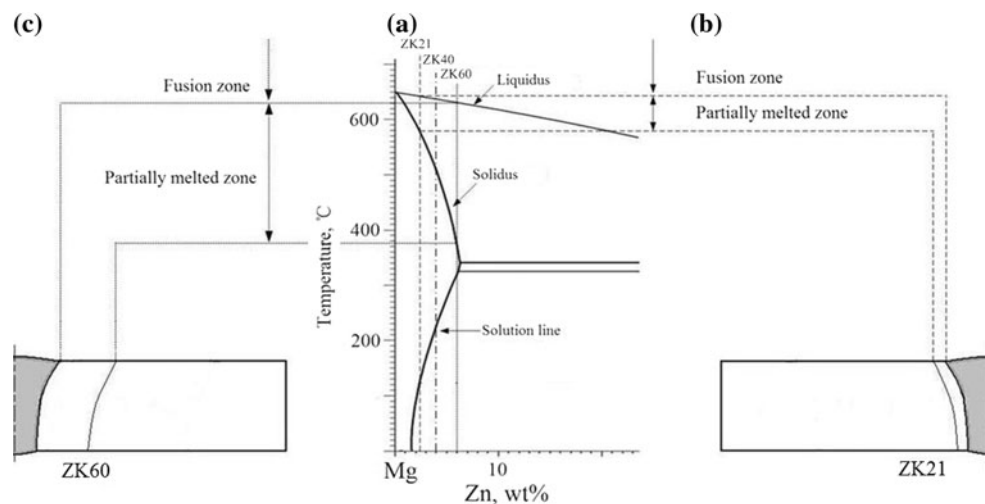


Fig. 3 **a** The Mg–Zn phase diagram [14], **b** sketch of ZK21 welded joint, and **c** sketch of ZK60-welded joint



liquation also occurs in the grain interior. Figure 3 gives the magnesium-rich portion of the Mg–Zn phase diagram [14] and the PMZ sketch of the laser beam-welded joints of ZK series magnesium alloys. From the phase diagram, the wider

solidification temperature range and the lower melting temperature of the Mg–Zn alloy are associated with the higher Zn content. For the ZK alloys, the solidification temperature ranges of ZK21, ZK40, and ZK60 are about

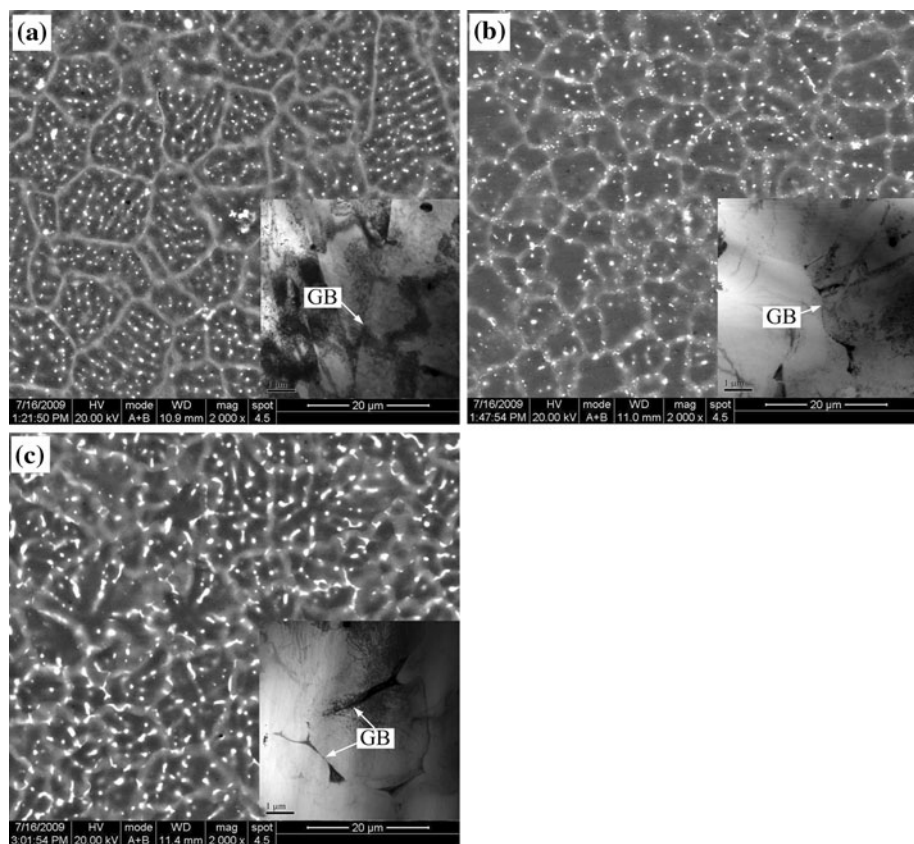
65 °C(580–650 °C), 135 °C(510–645 °C), and 265 °C(375–640 °C), respectively. The solid–liquid temperature interval of these alloys is sharply widened with increasing Zn content. Therefore, no visible PMZ is observed in ZK21, but a wider one with extensive liquation is detected in ZK60. It can be ascribed to the relatively narrow solid–liquid interval and the high temperature gradient in LBW for ZK21 [5]. The extent of liquation in PMZ can be reduced by reducing the Zn content of base metal.

As seen from Fig. 2a, the grains in fusion zone (FZ) adjacent to the fusion boundary of ZK21 show the characteristic of cellular grains, whereas those in FZ of ZK40 and ZK60 are both equiaxed dendrites shown in Fig. 2c and e. It is suggested that the different morphologies of grains are caused by the Zn content variation. According to the theory of welding metallurgy [15], the solidification mode in FZ is influenced by the solute content of the molten weld metal, the temperature gradient (G) in the direction of solidification and the growth rate (R) of the solidification front. For any given solidification parameter (G/R), the solidification mode may change from planar to cellular, to columnar dendritic and finally to equiaxed dendritic with increasing solute content. In fact, G and R are determined by heat input and the welding speed during the welding process. In this study, the laser power and the welding speed are constant, and thus the grain morphology

near the fusion boundary is determined only by the Zn content of the base metal. This explains well the differences of grains morphology in FZ adjacent to the fusion boundary between ZK21 and the latter two alloys.

The microstructures in FZ center of the three alloys are shown in Fig. 2b, d, and f respectively. It can be seen that all the grains exhibit homogeneously equiaxed dendrites but vary in size among the three alloys. The average grain sizes in FZ of ZK21, ZK40, and ZK60 are $11.5 \pm 0.5 \mu\text{m}$, $4.8 \pm 0.3 \mu\text{m}$, and $16.4 \pm 0.8 \mu\text{m}$, respectively, which was determined by linear intercept method. It has been reported that the effect of solute's content on the grain size in FZ mainly lies in two aspects [15]. As the solute's content increases, the grains can be coarsened by the longer solidification time due to the widening solidus–liquidus temperature interval, but refined by the intensified constitutional supercooling of molten weld metal. As the Zn content increases from 2.3 to 4 wt%, i.e., ZK21 to ZK40, the grain refinement effect is greater than the coarsening effect. Thus, the grain size of ZK40 is finer than that of ZK21. However, as the Zn content further increases from 4 to 6 wt%, i.e., ZK40 to ZK60, the difference of the solidification temperature range between them is higher than 120 °C, which leads to a longer solidification time of the molten weld metal. Therefore, the grain refinement effect of the constitutional supercooling enhancement is much

Fig. 4 The precipitates in FZ of the alloys: **a** ZK21, **b** ZK40, and **c** ZK60



weaker than the grain coarsening effect, and the grains are severely coarsened in FZ of ZK60. Evidently, the grains in FZ of ZK40 are the finest among the three alloys. It is indicated that finer grains in the FZ can be obtained by an appropriate Zn content in base metal, such as 4 wt% Zn (ZK40) in this study.

Figure 4 shows the SEM and TEM images for the FZ of the three alloys. For ZK21, as seen in Fig. 4a, a large amount of precipitates mainly distribute within the grains,

and no apparent precipitates along GBs can be found. For ZK40, as shown in Fig. 4b, the precipitates can be observed both within grains and along GBs. Compared to ZK40, more precipitates are observed along GBs in ZK60 and some of them are of larger sizes and with net-like forms (Fig. 4c). Using image analysis method, the volume fraction of the precipitates in ZK21, ZK40, and ZK60 are measured to be about 3.3, 3.6, and 8.6%, respectively. The mean particle diameters in the alloys are about 0.32, 0.35, and 0.74 μm , respectively. Evidently, it can be seen that the Zn content has a great influence on the size and distribution of the precipitates in FZ. This is mainly caused by the difference of dendrite arms growth and the different amounts of Zn segregation in the spaces between the arms. The growth of dendrite arms is dependent on the degree of the constitutional supercooling and the solidification time, which are closely associated with Zn content [15]. Most previous investigations have suggested that the net-like precipitates along GBs always weaken the strength of weld metal [5]. Further, XRD (Fig. 5a) and EDS analyses (Fig. 5b) show that the precipitates in FZ of ZK60 are $\text{Mg}_{51}\text{Zn}_{20}$ phase (Immm, orthorhombic crystal structure with $a = 1.4083 \text{ nm}$, $b = 1.4486 \text{ nm}$, and $c = 1.4025 \text{ nm}$) with a low melting point [16].

Mechanical properties of the welded joints

The mechanical properties of the welded joints are listed in Table 2. The average UTS of the base metals and the joints are shown in Fig. 6. It is obvious that the Zn content has also significant effects on the mechanical properties of the joints. The joint efficiencies (based on UTS) of ZK21 and ZK40 are higher than 90%, while it sharply reduces for ZK60. The joints of ZK40 possess the highest average ultimate tensile strength (UTS) of 312 MPa and good elongation of 6.4%, which are up to 90.4 and 56% of those of the base metal, respectively. In general, magnesium alloys with the Zn content higher than 2 wt% are difficult to be welded by arc welding due to solidification cracking

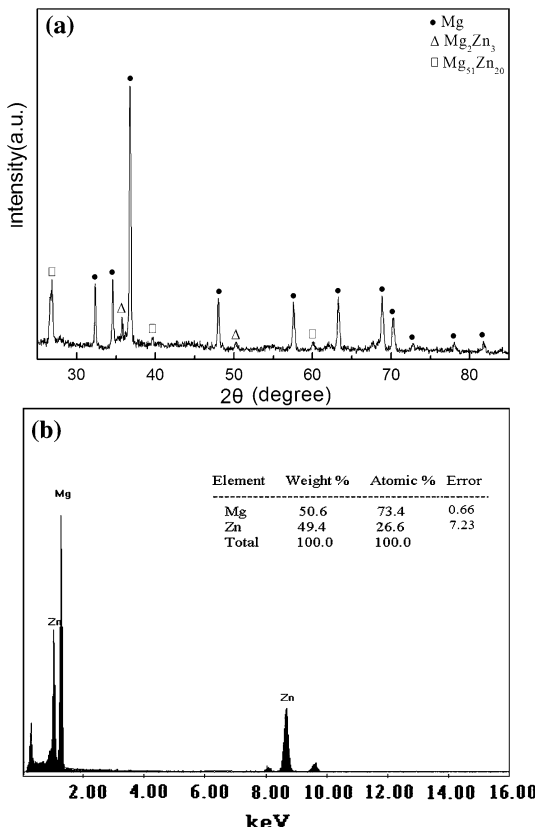


Fig. 5 a XRD pattern of ZK60 weld, b EDS analysis results of the precipitates along GBs in FZ of ZK60

Table 2 Mechanical properties of the welded joints in the ZK series alloys

Alloy	Tensile sample	σ_b (MPa)	σ_s (MPa)	σ_s/σ_b	δ (%)	Joint efficiency (%)
ZK21	1	279	211	0.76	5.7	91
	2	287	201	0.7	5.7	93
	3	289	216	0.75	5.1	94
ZK40	1	310	260	0.84	6.0	90
	2	310	255	0.82	6.5	90
	3	315	262	0.83	6.7	91
ZK60	1	260	182	0.70	3.8	72
	2	228	160	0.75	3.4	63
	3	256	180	0.70	5.0	71

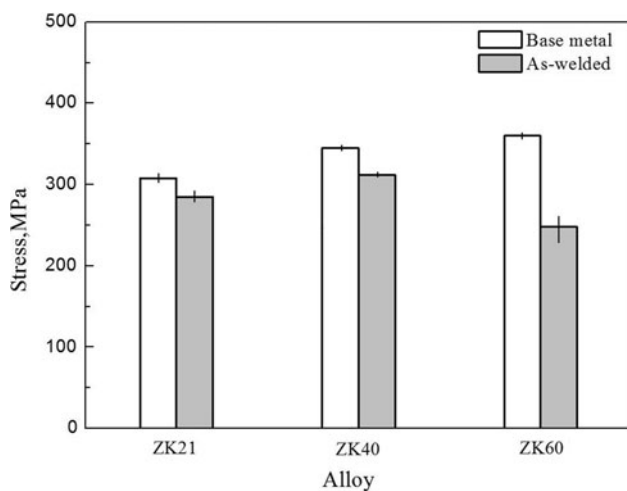


Fig. 6 Comparison of the average UTS of the base metals and the welded joints

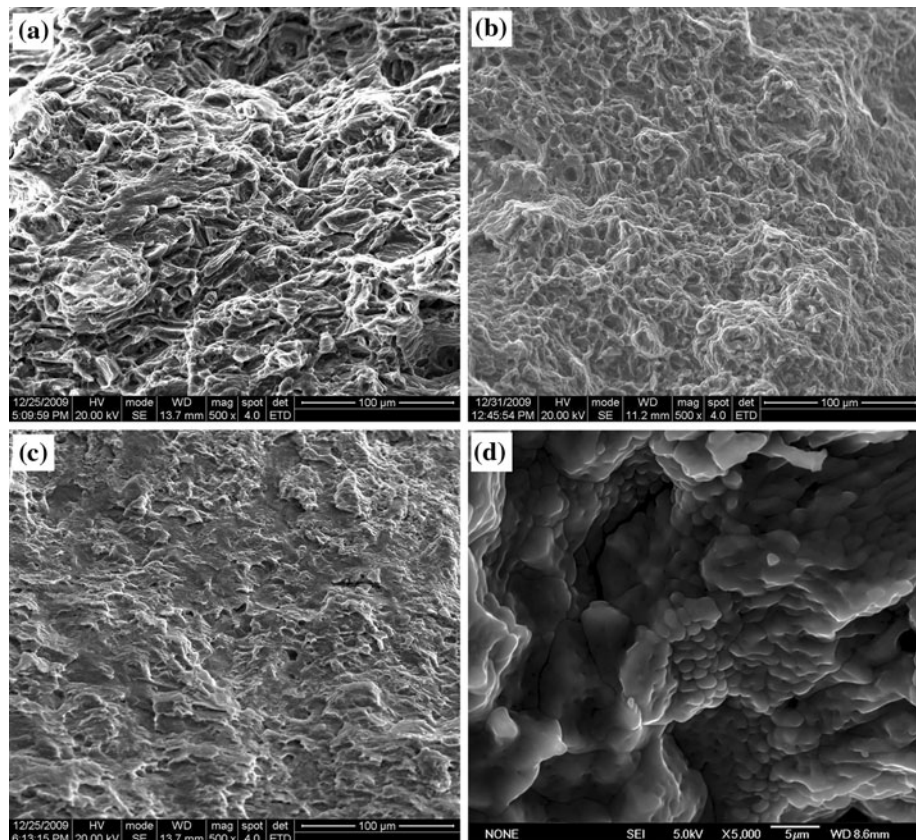
susceptibility [5]. However, a sound bead of ZK40 is obtained by LBW performed in this study. Therefore, it can be confirmed that LBW is suitable to weld ZK series magnesium alloys with Zn content up to 4 wt%.

Tensile test indicates that the fracture of the three alloys always occurs within the FZ, and the typical SEM

fractographs are presented in Fig. 7a–c. As seen from Fig. 7a, the fracture of ZK21 is characteristic of quasi-cleavage. There are several tearing ridges in the local positions, and some dimples can also be clearly observed. Therefore, it can be concluded that there is a mixed fracture mode for the ZK21. As seen from Fig. 7b, a large number of dimples can be observed in ZK40 which means the fracture is characteristic of ductility. However, ZK60 exhibits cleavage fracture (Fig. 7c). The fracture surface of sample 2 (Table 2) of ZK60-welded joint is shown in Fig. 7d. It can be seen that fracture is intergranular and its surface reflects the weld solidification structure, indicating that solidification cracking has occurred during welding. As mentioned above, a great amount of $Mg_{51}Zn_{20}$ precipitating along GBs weakens the weld metal. During the terminal stage of solidification, solidification cracking occurs when the tensile stress, originating from solidification shrinkage and thermal contraction, exceeds the strength of the almost completely solidified weld metal [17].

Microhardness testing is also conducted on the cross section of the joints. From Fig. 8, the microhardness values for the heat-affected zone (HAZ) and the base metals increase with increasing Zn content. The HAZ annealing softening can be observed in these alloys. The closer to the

Fig. 7 SEM fractographs of the joints: **a** ZK21, **b** ZK40, **c** ZK60, and **d** portion of fracture surface for sample 2 in LBW ZK60



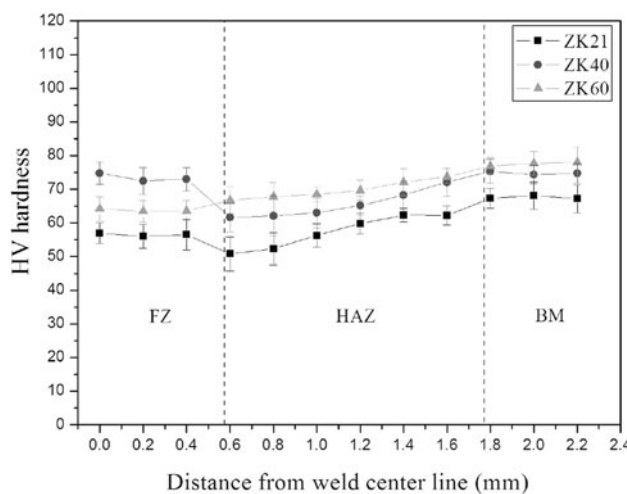


Fig. 8 The hardness profiles of the joints

fusion boundary, the higher the peak temperature becomes and the longer the metal stays above the effective recrystallization temperature. Thus, the grains in the HAZ become coarsening as the fusion boundary approaching [17]. Noticeably, the microhardness values in FZ of ZK40 are the highest among the three alloys, which may originate from the finer grains.

Conclusions

In this study, the as-rolled ZK21, ZK40, and ZK60 magnesium alloy sheets are welded using a 3.0-kW CO₂ laser beam, and the effects of Zn content on the microstructures and mechanical properties are studied. The main conclusions are drawn as follows:

1. The LBW is suitable for ZK21- and ZK40-welded magnesium alloys. However, ZK60 is susceptible to solidification cracking and presents a poor weldability, which may originate from the net-like distribution of more Mg₅₁Zn₂₀ precipitates along GBs in the FZ.
2. With Zn content increasing, the amount and mean size of precipitates along GBs in the FZ increase, and the

morphology of grains in the FZ adjacent to fusion boundary changes from cellular to equiaxed dendritic.

3. The grain size in the FZ is influenced by Zn content of base metal. The finest grain can be obtained in the FZ of ZK40-welded joint, the size of which is only about 4.8 μm; the ZK40-welded joint achieves the highest tensile strength of 312 MPa up to 90.4% of the base metal.

Acknowledgements The research study described in this article was supported by the Program for New Century Excellent Talents in University of Ministry of Education of China (NCET-06-0701).

References

1. Liu LM, Qi XD (2009) J Mater Sci 44:5725. doi:[10.1007/s10853-009-3797-9](https://doi.org/10.1007/s10853-009-3797-9)
2. Liu LM, Song G, Zhu ML (2008) Mater Trans A 39:1702
3. Zhang ZD, Liu LM, Sun H, Wang L (2008) J Mater Sci 43:1382. doi:[10.1007/s10853-007-2299-x](https://doi.org/10.1007/s10853-007-2299-x)
4. Wang CY, Wang XJ, Chang H, Wu K, Zheng MY (2007) Mater Sci Eng A 464:52
5. Kearns WH (1982) Welding handbook, vol 4. American Welding Society, Miami
6. Cao X, Rivaux B, Jahazi M, Cuddy J, Birur A (2009) J Mater Sci 44:4557. doi:[10.1007/s10853-009-3691-5](https://doi.org/10.1007/s10853-009-3691-5)
7. Venkateswaran P, Xu ZH, Li XD, Reynolds AP (2009) J Mater Sci 44:4140. doi:[10.1007/s10853-009-3607-4](https://doi.org/10.1007/s10853-009-3607-4)
8. Zhang Z, Chen JT (2008) J Mater Sci 43:222. doi:[10.1007/s10853-007-2129-1](https://doi.org/10.1007/s10853-007-2129-1)
9. Coelho RS, Kostka A, Pinto H, Riekehr S, Kocak M, Pyzalla AR (2008) Mater Sci Eng A 485:20
10. Zhu JH, Li L, Liu Z (2005) Surf Sci 247:300
11. Quan YJ, Chen ZH, Yu ZH, Gong XS, Li M (2008) Mater Charact 59:1799
12. Baeslack WA III, Savage SJ, Froes FH (1986) J Mater Sci Lett 5:935
13. Cao X, Xiao M, Jahazi M, Immarigeon JP (2005) Mater Manuf Process 20:987
14. Anderson MM, Baker H (1999) ASM specialty handbook: magnesium and magnesium alloys. ASM International, Materials Park
15. Lancaster JF (1999) Metallurgy of welding. Woodhead, Cambridge
16. Higashi I, Shiotani N, Uda M, Mizoguchi T, Katoh H (1981) J Solid State Chem 36:225
17. Kou S (2002) Welding metallurgy. Wiley-Interscience, Hoboken